Journal of Proteomics 151 (2017) 193–203

Contents lists available at ScienceDirect

Journal of Proteomics

journal homepage: www.elsevier.com/locate/jprot

Understanding global changes of the liver proteome during murine schistosomiasis using a label-free shotgun approach

Jonatan Marques Campos [a,b], Leandro Xavier Neves [b], Nívia Carolina Nogueira de Paiva [c], Renata Alves de Oliveira e Castro [d], Ana Helena Casé [b], Cláudia Martins Carneiro [e], Milton Hércules Guerra Andrade [f], William Castro-Borges [f,*]

[a] Programa de Pós Graduação em Bioengenharia, Universidade Federal de São João del Rei, São João del Rei, MG, Brazil
[b] Programa de Pós Graduação em Biotecnologia, Universidade Federal de Ouro Preto, Ouro Preto, Minas Gerais, Brazil
[c] Núcleo de Pesquisas em Ciências Biológicas, Universidade Federal de Ouro Preto, Ouro Preto, Brazil
[d] Programa de Pós Graduação em Ciências Biológicas, Universidade Federal de Ouro Preto, Ouro Preto, Minas Gerais, Brazil
[e] Departamento de Análises Clínicas, Universidade Federal de Ouro Preto, Ouro Preto, Minas Gerais, Brazil
[f] Departamento de Ciências Biológicas, Núcleo de Pesquisas em Ciências Biológicas, Universidade Federal de Ouro Preto, Ouro Preto, Minas Gerais, Brazil

ARTICLE INFO

Article history:
Received 1 February 2016
Received in revised form 3 July 2016
Accepted 11 July 2016
Available online 15 July 2016

Keywords:
Schistosoma mansoni
Schistosomiasis
Liver biomarkers
Label-free
Shotgun proteomics

ABSTRACT

Schistosomiasis is an endemic disease affecting over 207 million people worldwide caused by helminth parasites of the genus Schistosoma. In Brazil the disease is responsible for the loss of up to 800 lives annually, resulting from the desabilitating effects of this chronic condition. In this study, we infected Balb/c mice with *Schistosoma mansoni* and analysed global changes in the proteomic profile of soluble liver proteins. Our shotgun analyses revealed predominance of up-regulation of proteins at 5 weeks of infection, coinciding with the onset of egg laying, and a remarkable down-regulation of liver constituents at 7 weeks, when severe tissue damage is installed. Representatives of glycolytic enzymes and stress response (in particular at the endoplasmic reticulum) were among the most differentially expressed molecules found in the infected liver. Collectively, our data contribute over 70 molecules not previously reported to be found at altered levels in murine schistosomiasis to further exploration of their potential as biomarkers of the disease. Moreover, understanding their intricate interaction using bioinformatics approach can potentially bring clarity to unknown mechanisms linked to the establishment of this condition in the vertebrate host.

Significance: To our knowledge, this study refers to the first shotgun proteomic analysis to provide an inventory of the global changes in the liver soluble proteome caused by *Schistosoma mansoni* in the Balb/c model. It also innovates by yielding data on quantification of the identified molecules as a manner to clarify and give insights into the underlying mechanisms for establishment of Schistosomiasis, a neglected tropical disease with historical prevalence in Brazil.

1. Introduction

Schistosomiasis is an endemic disease affecting over 207 million people worldwide [1]. It is considered by the World Health Organization to be the second most important parasitic disease due to its social and economical impact, leading to an estimated 200,000 deaths annually [2]. In Brazil, although levels of prevalence and morbidity have declined over the years, the disease still accounts for 700–800 deaths annually [3]. Therefore, early and sensitive diagnosis as well as the identification of biomarkers of the disease are of major public health interest.

Whilst assessing the course of Schistosomiasis in the human host is a difficult task, the laboratory mouse offers a convenient and fast manner to understand the underlying mechanisms that leads to, in particular, liver pathology. Previous studies have demonstrated the proteomic alterations in murine CBA/J strain liver schistosomiasis by means of two-dimensional gel electrophoresis, a classic proteomic approach [4,5]. A number of differentially proteins have been elucidated including cytokeratin 18 now proposed as a biomarker of the disease [6]. Metabolomic studies have also shed light on key metabolic alterations associated to the disease [7,8].

Here we interrogated quantitatively the soluble liver proteome of Balb/c infected mice using a label-free shotgun analysis. Such global analysis allowed observation of two distinct stages of the infected liver each characterized by 1) up-regulation of constituents coinciding with the onset of egg laying and 2) massive down-regulation of proteins as a testimonial of irreversible liver damage during late hepatosplenic schistosomiasis. Our findings contributed to reveal a further 81

* Corresponding author.
E-mail address: williamcborges@hotmail.com (W. Castro-Borges).

http://dx.doi.org/10.1016/j.jprot.2016.07.013
1874-3919/

molecules not previously reported to be differentially expressed in murine schistosomiasis, providing additional data to explore potential biomarkers of the disease. Altogether, our data pave the way to novel molecular insights into the underlying cellular mechanisms required for establishment of the chronic liver pathology caused by *S. mansoni*.

2. Material and methods

2.1. Ethics statement

The routine procedures for maintenance of the *S. mansoni* life cycle were reviewed and approved by the local Ethics Committee on Animal Experimentation, 'Comissão de Ética no Uso de Animais (CEUA)', Universidade Federal de Ouro Preto (UFOP), protocol n°. 2011/55.

2.2. Mice infection and experimental groups

Forty female Balb/c mice aged 30 days and of approximately 20 g weight were anesthetised using a combination of ketamine hydrochloride and xylazine, administered intraperitoneally at 8 mg/kg and 4 mg/kg, respectively. Subsequently, the animals were separated into four groups of 10 animals each. Two of these groups had their animals infected by *S. mansoni* larvae (LE strain) at a dose of 200 cercariae/animal, through active penetration via their previously shaved abdominal skin [9]. The remaining animals were submitted to a similar procedure, in which the cercarial suspension was replaced by tap water; these represented the two control groups. Infected and control animals were weighted and then euthanised at the 5th and 7th weeks post infection, to provide biological material from both splenic and hepatosplenic schistosomiasis, respectively. In the two occasions, approximately 700 μL of blood was drawn by cardiac puncture prior to perfusion of the hepatic portal system using saline citrate solution (0.85% NaCl, 0.75% sodium citrate), essentially as described [10]. Livers and spleens were collected, weighed and then washed in phosphate buffered solution (PBS 0.01 M pH 7.2). Liver sections of approximately 0.5 cm^2 were stored in 3.7% buffered-formalin pH 7.2 for subsequent histological analyses. The remaining sections were frozen at −80 °C for proteomic studies.

2.3. Distinguishing acute from chronic phase schistosomiasis in the murine model

To distinguish between acute and chronic phase schistosomiasis in the mouse model, a number of parameters were evaluated. The onset of oviposition was investigated by parasitological examination of faeces of all infected animals from 35th to 50th days post infection. The percentage ratios *liver-to-body weight* and *spleen-to-body weight* (% organ/body) were calculated to assess the level of hepatosplenomegaly, as suggested by [11]. Global and differential leukocyte counts were also obtained. These parameters alongside the histological analyses allowed us to differentiate acute from chronic liver disease.

2.4. Histological analysis

Liver sections were fixed in 3.7% buffered formalin pH 7.2 and embedded in paraffin. Tissue sections of approximately 4 μm thick were obtained using a microtome followed by staining the slides with hematoxylin & eosin (HE) and Masson's Trichrome. Quantitative evaluations of the number of inflammatory cells were performed in the hepatic perivascular region from control and infected animals.

2.5. Sample preparation

Soluble liver proteins were obtained from 100 mg of tissue. Firstly, the frozen sections were subjected to a maceration step in liquid nitrogen and resuspension of the ground material in 1 mL 25 mM Tris-HCl pH 7.5 containing 1× protease inhibitor cocktail (Sigma Aldrich, St. Louis, USA). The samples were homogenized by sonication (Branson Sonifier 250) using 5 cycles of 20 pulses each in an ice bath. The resulting suspension was centrifuged at 50,000 ×*g* for 2 h, at 4 °C followed by recovery of the supernatant containing the soluble proteins. Protein content was assessed using PIERCE™ BCA Protein Assay Kit (Thermo Scientific, Rockford, USA).

2.6. In solution digestion

Thirty microgram aliquots of soluble liver proteins obtained from pooled samples of three animals were reduced using 2 mM dithiothreitol (Sigma Aldrich) in 100 mM ammonium bicarbonate at 56 °C, for 15 min. Proteins were alkylated in 4.5 mM iodoacetamide (Sigma Aldrich) for 15 min in the dark. After alkylation the samples were diluted 1:1 in 100 mM ammonium bicarbonate and digested at 37 °C for 12 h using Sequencing Grade Modified Trypsin (Promega, Madison, USA) at a ratio of 25:1(protein/trypsin). Trypsin activity was stopped by addition of 4% (*v*/v) ultra-pure glacial acetic acid (J.T. Baker, Center Valley, USA). Peptide mixtures were cleaned up using a Strata C18-E cartridge (55 μm, Phenomenex, Macclesfield, UK) and dried in a *speed vacuum* equipment for sequential analyses by mass spectrometry.

2.7. LC-MS/MS

Three micrograms of peptides were separated on a UltiMate® 3000 nano UHPLC system (Thermo Scientific, Bremen) set up with an Acclaim PepMap100 C18 Nano-Trap Column (75 μm i.d. × 2 cm, 3 μm, 100 Å; Thermo Scientific) in line with an Acclaim PepMap100 C18 RSLC capillary column (75 μm i.d. × 15 cm, 2 μm, 100 Å; Thermo Scientific). Peptides were previously washed with 2% acetonitrile/0.05% trifluoroacetic acid for 3 min and separated at 40 °C using a non-linear solvent gradient, A (0.1% formic acid) and B (80% acetonitrile/0.1% formic acid). The gradient varied from 4–30% solvent B in 120 min and 30–55% at 40 min. Finally, the gradient changed from 55 to 90% solvent B in 10 min and a finishing step in 4% solvent B for 10 min. Spectra scans were acquired in Q-Exactive™ mass spectrometry instrument (Thermo Scientific), coupled to nano UHPLC system via a nanoelectrospray ion source. The instrument operated in 2.8 kV, positive mode, resolution of 70,000 at range of 300–2000 *m/z*, maximum injection time of 100 ms and target value of $3e^6$ ions. Up to 12 most intense precursors ions with charge state ≥2 were isolated from a 2 *m/z* window and fragmented via higher-energy collisional dissociation - HCD (collision energy of 30 V). MS/MS spectra were acquired with resolution of 17,500 with maximum injection time of 150 ms and target value of $2e^5$ ions. Dynamic exclusion was set to 60 s.

2.8. Data processing

The .raw files obtained from the Q-Exactive instrument were submitted to database searching using the MaxQuant® software, version 1.5.2.8 [12]. Protein identification was performed against a UniProt *Mus musculus* reviewed compilation containing 16,686 sequences. Identification parameters were as follows: N-terminal acetylation and oxidation of methionine were considered as variable modifications. Tripsyn/P was set as the digestion enzyme and a maximum of two missed cleavages were allowed. Orbitrap was assigned as the instrument type and peptide tolerance set to 4.5 ppm. Other parameters included: isotope match tolerance (2 ppm), minimum peak length (2), and maximum charge state (+7). Relative abundance of proteins were obtained using Label-Free Quantification (LFQ) provided by the maxLFQ intensity data using the default mode [13]. The global parameters were selected as re-quantify and match between runs. False Discovery Rate (FDR) and Peptide Sequence Match (PSM) were 0.01, minimum peptide length 7 and minimum razor + unique peptide was set to 1. The parameter decoy was activated in revert mode and

the option of a second peptide was used to reduce loss of co-eluting peptides.

The Skyline software was used to validate a set of proteins revealed as upregulated in both infected groups by MaxQuant. The proteins cytokeratins 8 and 18, calreticulin, endoplasmin and L-lactate dehydrogenase were validated using the MS1 filtering tool and data analysis features available on Skyline 3.5 [14] (freely downloaded at http://proteome.gs.washington.edu/software/skyline). Initially, a comprehensive spectral library was built in Skyline with all peptide-spectrum matches assigned by Andromeda at a cut-off score of 0.95. All tryptic peptides used for quantification in Skyline obeyed the following criteria: 7–16 amino acids in length; absence of both missed cleavages and methionine residues; no PTM other than cysteine carbamidomethylation was accepted. The extracted ion-chromatograms were obtained within a 5 min window and multiply-charged peptides had only the most intense ion analysed.

2.9. Statistical analysis

In order to evaluate the reproducibility achieved among the various chromatographic separations a correlation statistics (Spearman's) test was performed for each of the three biological replicates from control and infected animals. Only runs displaying correlation coefficients ranging from 0.85 to 1 were included in this study. Data on relative abundance obtained through MaxQuant® software (maxLFQ) were analysed by Multiple-*t*-test using GraphPad Prism 6.00, San Diego, California, USA. Proteins exhibiting at least two maxLFQ data among the triplicates were considered for statistical analysis. A volcano plot was produced using the maxLFQ ratio (infected/control) against all p-values obtained for the identified proteins to assess their pattern of up- or downregulation. Among these, only the ones that exhibited significance ($p \leq 0.05$) were considered statistically different comparing control and infected animals.

2.10. Protein categorization and protein-interaction network

Protein annotation were obtained from UniProtKB and categorized by Gene Ontology process (GO) based on the molecular function (MF), biological process (BP), and cellular component (CC). The STRING v10.0 database (http://string-db.org) was used to generate protein-protein network maps to visualize possible interactions for proteins of interest [15].

3. Results

3.1. Establishment of acute and chronic schistosomiasis in the murine model

The use of different approaches to differentiate acute from chronic schistosomiasis in the murine model, allowed us to obtain biological material from two distinct stages of the disease. The monitoring of oviposition by parasitological examinations showed a significant increase in the number of eggs present in the faeces of infected animals. As shown in Supplemental Fig. 1, eggs were scarcely detected up to 40 days of infection. In contrast, a five-fold increase in the number of detected eggs was observed on the 45th day post infection, with that number increasing to a 100% on the 50th day. The percentage ratios *liver-to-body weight* and *spleen-to-body weight* also revealed two distinct stages of the disease comparing 5 and 7 weeks post infection. Whilst a pronounced increased in the spleen was observed at the 5th week, a very small but significant increase in the liver weight of infected animals was detected in the same period. In stark contrast, at the 7th week post infection both liver and spleen were largely increased in the infected animals, Supplemental Fig. 2. Histopathological and morphometric analyses revealed inflammatory infiltrates in the perivascular region of the liver for both time points, with a pronounced increase (approx. 100%) in the number of cells at 7 weeks of infection, Supplemental Fig. 3.

3.2. There is a significant change in soluble liver proteome of mice infected with S. mansoni

Our shotgun proteomic analysis allowed confident identification of 764 soluble liver proteins using the Maxquant® as the searching algorithm, Supplementary Table 1. The reproducibility of the biological triplicates obtained from control and infected livers was assessed by a Spearman correlation, using LFQ intensity data. As shown in Supplemental Fig. 4, correlation coefficients ranged from 0.92 to 0.98 for control mice and from 0.87 to 0.92 for infected animals, attesting for the intrinsic homogeneity of the soluble preparations further subjected to comparisons. Then, by applying stringent criteria for measuring the relative abundance of liver proteins from control and infected animals, we were able to quantify respectively, 174 and 164 molecules that exhibited either up or downregulation of expression at 5 and 7 weeks post infection, Fig. 1 and Supplementary Table 2. The liver soluble proteome of mice at the 5th week of infection revealed a total of 93 proteins significantly upregulated ($p \leq 0.05$) and only one protein significantly downregulated, Fig. 1A. The vast majority of up-regulated molecules represented 53.4% of the quantifiable proteins found in this group. A contrasting pattern of protein expression was observed in 7th week infected mice. In those animals, only 10 proteins appeared upregulated whilst 51 were downregulated, totaling 61 altered proteins, representing 37.2% of the quantifiable proteins in this group, Fig. 1B. This marked change in protein profile comparing splenic and hepatosplenic schistosomiasis corroborates with our histological findings. The hepatic parenchyma of the 5th week infected animals displayed a reduced number of only immature eggs and the initial recruitment of an inflammatory infiltrate, Fig. 1C. In contrast, an equivalent hepatic section, from the 7th week infected animal, is dominated by an intense granulomatous inflammation surrounding eggs present at much later stages of development, Fig. 1D.

3.3. Few protein categories remains significantly expressed in chronic liver schistosomiasis

All differentially expressed proteins ($p \leq 0.05$) were classified according to their biological functions (GO), in 17 distinct categories. At the 5th week post infection, from the 94 proteins significantly altered in the liver, over 70% were classified in the following categories: amino acid metabolism (19); stress (11); chaperone (10); lipid metabolism (8); carbohydrate metabolism (7), structural (6), and signaling (6), Fig. 2A and Table 1. Glutamate dehydrogenase 1 (+2.40 fold) and Carbamoyl-phosphate synthase (+2.39 fold) were the two enzymes showing the highest fold increase in the amino acid metabolism category. Alcohol dehydrogenase 1 (+2.59 fold) and Peroxiredoxin-5 (+2.39) were abundant representatives of stress proteins. Among the quantified chaperones, calreticulin showed the highest increase (+2.33 fold). In the lipid metabolism category, NADPH: adrenodoxin oxidoreductase (+3.94 fold) and medium-chain acyl-CoA dehydrogenase (+2.28 fold) merited attention. In the same category, acyl-CoA binding protein represented the only molecule significantly downregulated at the 5th post infection. L-lactate dehydrogenase A chain (+2.28 fold) and Pyruvate carboxylase (+2.16 fold) were the two major representatives within carbohydrate metabolism. In the group of structural proteins, cytokeratin 18 (+2.76 fold), isoform 2 of tropomyosin alpha-3 chain (+2.70 fold) and cytokeratin 8 (+2.30 fold) exhibited high expression levels. Within signaling, two isoforms of 14-3-3 proteins, calumenin and phosphatidylethanolamine-binding protein displayed over 2 fold increase in expression.

At the 7th week post infection, out of 61 proteins, 51 were found to be downregulated whilst 10 were upregulated. The major categories of proteins significantly upregulated after 7 weeks of infection were:

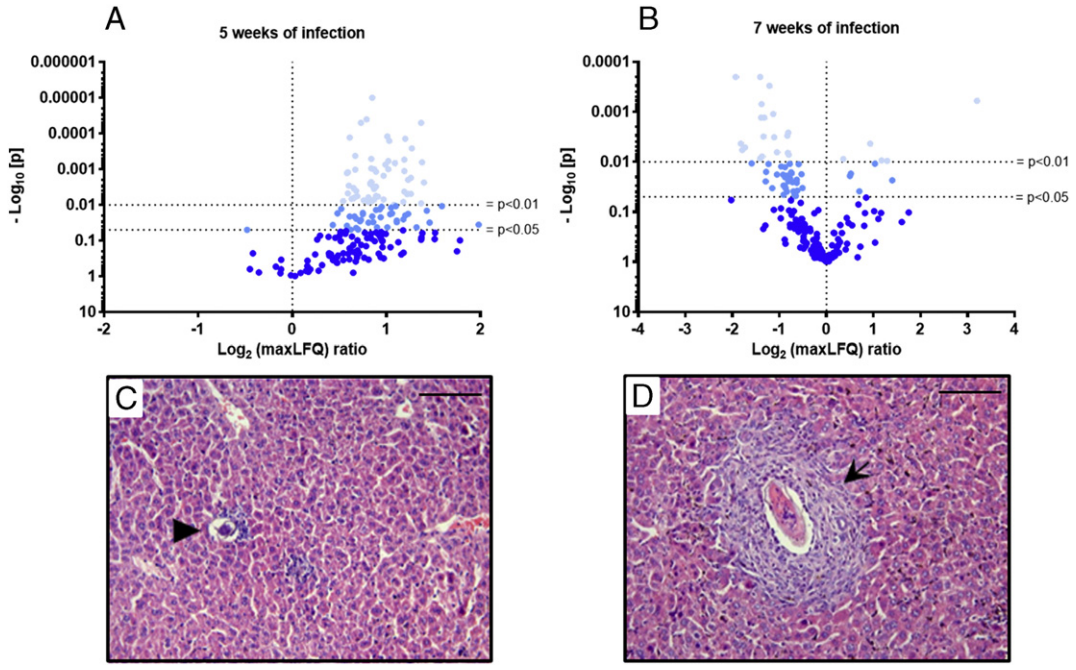

Fig. 1. Splenic and hepatosplenic schistosomiasis in the Balb/c model are associated to major differences in the proteome profile of soluble liver proteins. A – The Volcano plot revealed predominantly up-regulation of liver proteins at 5 weeks of infection. B – In contrast, at 7 weeks of infection the liver soluble proteome is dominated by down-regulation of proteins. C – Immature egg of *S. mansoni* located in the liver parenchyma of mice at 5 weeks of infection, surrounded by a moderate inflammatory process (arrow head). D – Mature *S. mansoni* egg located in the liver parenchyma at 7 weeks of infection, surrounded by an intense granulomatous inflammation (arrow). The photomicrographs shown here remind the major tissue alterations seen in both stages of the disease. Note the large area occupied by granuloma formation at 7 weeks of infection, causing a considerable loss of functional hepatic tissue. Hematoxylin-eosin staining (c–d); Bar = 100 μm.

structural (3), chaperones (3), amino acid metabolism (1), signaling (1) and translation (1), Fig. 2B and Table 1. Structural proteins and chaperonins were the most upregulated at 7 weeks of infection. Three structural proteins that increased in abundance were profilin-1(+2.63 fold), cytokeratin 8 (+2.45 fold) and cytokeratin 18 (+2.04 fold). Chaperones constituted another class of proteins that persisted at increased levels up to the 7th week of infection. These included calreticulin (+2.25 fold), endoplasmin (+1.90 fold) and HSP 90-beta (+1.41 fold). Four other proteins showed significantly increased abundance, these were gamma-glutamyltransferase (+9.16 fold – aminoacid metabolism), lactate dehydrogenase (+1.63 fold – carbohydrate metabolism), inositol monophosphatase 1(+1.28 fold – signaling) and elongation factor 2 (+1.43 fold – translation).

3.4. Five liver proteins remained significantly upregulated during splenic and hepatosplenic schistosomiasis

All proteins significantly altered in the liver of mice at the 5th and 7th week of infection, found to be up or downregulated, were examined using a Venn diagram in order to ease visualization of unique proteins found at each stage of the disease and those that were shared, Fig. 3A. From a total 92 proteins upregulated at 5 weeks of infection, 56 proteins are uniquely upregulated at this stage whilst another 31 proteins exhibited downregulation after 7 weeks of infection. At 7th week of infection, 51 proteins were downregulated of which 20 proteins were identified solely at this stage of the disease. Only 10 proteins were upregulated at the 7th week of infection, of which five were uniquely found at this stage (γ-glutamyltransferase; heat shock protein HSP 90-beta; profilin-1; inositol monophosphatase-1 and elongation factor-2). The remaining five proteins maintained increased expression levels from the 5th week of infection onwards. These were represented by cytokeratin 8, cytokeratin 18, calreticulin, endoplasmin and L-lactate dehydrogenase, Fig. 3B. The persistently increased levels of these five proteins, during early and late chronic infection, were again confirmed and validated through another mass-spectrometric approach provided by the Skyline algorithm (Supplemental Fig. 5).

3.5. Protein interaction network

The three molecules (calreticulin, endoplasmin and L-lactate dehydrogenase) found at persistent high levels at the 5th and 7th week of infection, were selected for protein interaction network using the STRING algorithm. Further insights into novel interactors were gained by requesting the extra addition of the 20 most likely partners. KEGG pathway analysis of the resulting network revealed molecules involved in protein processing in the endoplasmic reticulum displaying the most prominent protein hubs (red nodes), Fig. 4. Other cellular pathways included antigen presentation, amino acid and carbohydrate metabolism.

4. Discussion

Here we aimed to quantitatively identify the alterations in the soluble liver proteome from *S. mansoni* infected-mice (Balb/c strain) using a large scale sequencing approach. In complement to previous studies, which pioneered similar investigation through use of 2-D electrophoresis and MALDI-TOF/TOF analysis for protein identification [4,6], here we made use of highly sensitive proteomic tools to expand the list of proteins playing specific roles in the murine model of liver schistosomiasis. Using stringent criteria of quantitation at the peptide level, we were able to confidently register minor variations in protein abundance comparing infected and non-infected livers. As previously reported, two distinct stages of the disease in the mouse model are of relevance. Firstly, splenomegaly develops without appreciable increase in the liver and, at the chronic phase, exacerbated hepatosplenomegaly is often observed [4,11]. The latter is also accompanied by intestinal disease due to the inflammation caused by parasite eggs [16]. These two distinct stages differ among various mice strains particularly concerning their timing and percentage of animals that end up exhibiting both disease states [5].

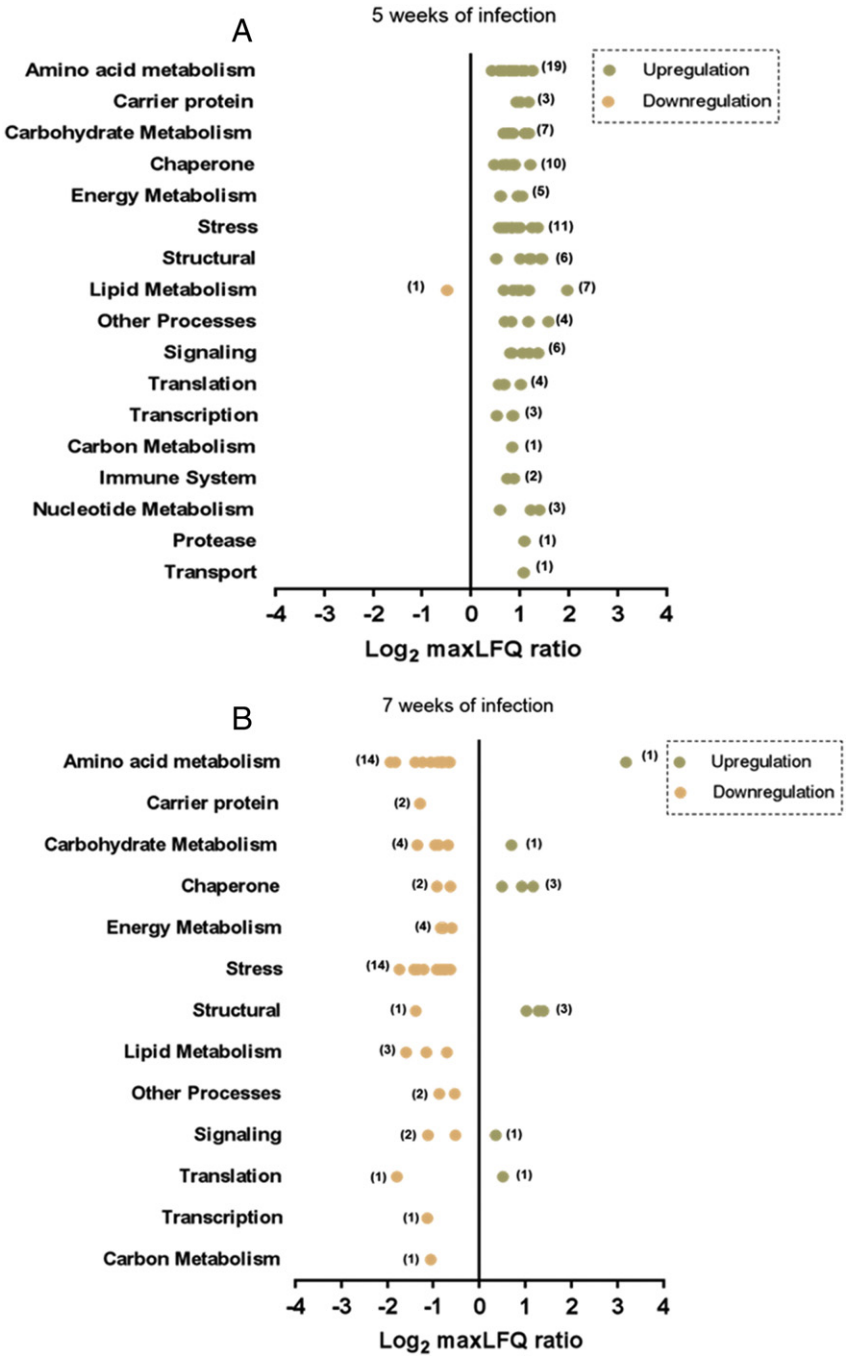

Fig. 2. Categorization of liver proteins significantly exhibiting up or down-regulation at 5 and 7 weeks of infection. Differentially expressed proteins ($p \leq 0.05$) were classified according to their biological functions, using Gene ontology (GO) and UniProtKB. A - Proteins differentially expressed at 5 weeks of infection were classified into 17 biological categories. B - At 7 weeks post infection the differentially expressed proteins were classified into 13 biological categories. Note the predominance of up-regulation for constituents of various protein categories at 5 weeks post infection and the opposite scenario observed at 7 weeks.

In this context, we first established the periods in which splenomegaly and hepatosplenomegaly would be best distinguished in the Balb/c strain. We have chosen 5 weeks of infection to investigate the proteomic alterations seen during the splenic phase as parasite eggs in the faeces were lower, the spleen was over 100% large and the liver-to-body ratio had just significantly differed from non-infected mice. In stark contrast, at 7 weeks post infection in this model, eggs were abundantly found in the faeces and both spleen-to-body and liver-to-body ratios greatly differed from control animals. These preliminary data on the characterization of the two stages of the disease were then corroborated by our histological findings which demonstrated major in situ differences in their inflammatory processes.

Large-scale protein analyses allow us to make a comparative measurement of many proteins simultaneously [17]. Identification of proteins present under varying dynamic ranges are greatly facilitated by increased resolution of chromatographic separations in parallel to high accuracy of mass analyzers [18,19]. Simultaneously, label-free proteomic approaches have been optimized to allow detection of small changes in protein abundance [20,21]. Here, we employed a label-free quantification method provided by the MaxQuant® algorithm [12,13]. A volcano plot allowed the observation that the majority of the identified liver proteins expressed at the splenic phase of the disease (5 weeks post infection) were upregulated. In total, 93 proteins exhibited significantly higher levels, 30 of which showing a minimum of 2 fold increase.

Table 1
Proteins significantly altered in the liver at the 5th and 7th week of infection.

ID UniProtKB	Protein name	5 weeks of infection Log_2 (maxLFQ ratio) Test/Control	5 weeks of infection p value	7 weeks of infection Log_2 (maxLFQ ratio) Test/Control	7 weeks of infection p value	Razor + unique peptides	Unique + razor sequence coverage [%]	Mol. weight [kDa]
Amino acid metabolism								
P26443	Glutamate dehydrogenase 1, mitochondrial	+1.27	0.0003	–	–	14	29.9	61.3
Q8C196	Carbamoyl-phosphate synthase, mitochondrial	+1.26	0.0017	−0.82	0.0066	62	50.1	164.6
O09173	Homogentisate 1,2-dioxygenase	+1.11	0.0274	−0.75	0.0161	6	22.0	50.0
P11725	Ornithine carbamoyltransferase, mitochondrial	+1.09	0.0007	−1.05	0.0178	6	17.2	39.8
O35423-2	Serine–pyruvate aminotransferase, mitochondrial[a]	+1.04	0.0180	−1.39	0.0013	6	19.9	43.5
P05202	Aspartate aminotransferase, mitochondrial	+0.93	0.0132	−0.65	0.0474	11	24.7	47.4
O09173	Homogentisate 1,2-dioxygenase	+0.91	0.0462	---	---	6	22.0	50.0
Q8QZR5	Alanine aminotransferase 1[a]	+0.91	0.0059	−0.88	0.0202	5	11.7	55.1
Q8VBT2	L-serine dehydratase/L-threonine deaminase[a]	+0.90	0.0421	−1.82	0.0043	3	15.3	34.6
Q78JT3	3-Hydroxyanthranilate 3,4-dioxygenase	+0.86	0.0301	−1.23	0.0110	5	21.7	32.8
O09172	Glutamate–cysteine ligase regulatory subunit[a]	+0.84	0.0023	---	---	2	10.2	30.5
P50431	Serine hydroxymethyltransferase, cytosolic[a]	+0.79	0.0000	---	---	7	16.1	52.6
Q8CHT0	Delta-1-pyrroline-5-carboxylate dehydrogenase[a]	+0.68	0.0041	−1.39	0.0157	8	18.3	61.8
P49429	4-hydroxyphenylpyruvate dioxygenase	+0.66	0.0062	−0.80	0.0072	10	32.1	45.1
P05201	Aspartate aminotransferase, cytoplasmic	+0.65	0.0033	−0.68	0.0474	8	25.4	46.2
P29758	Ornithine aminotransferase, mitochondrial[a]	+0.62	0.0489	---	---	5	15.3	48.4
Q71RI9-2	Isoform 2 of Kynurenine–oxoglutarate transaminase 3[a]	+0.59	0.0012	---	---	3	11.7	47.3
O35490	Betaine–homocysteine S-methyltransferase 1	+0.59	0.0047	---	---	9	31.9	45.0
P35492	Histidine ammonia-lyase[a]	+0.43	0.0364	---	---	4	7.80	72.3
P21981	Protein-glutamine gamma-glutamyltransferase	---	---	+3.20	0.0006	13	27.0	77.1
P16460	Argininosuccinate synthase	---	---	−0.63	0.0261	12	28.2	46.6
Q8VCN5	Cystathionine gamma-lyase[a]	---	---	−0.81	0.0026	7	24.9	43.6
P50247	Adenosylhomocysteinase	---	---	−0.91	0.0296	11	26.2	47.7
Q8VC12	Urocanate hydratase[a]	---	---	−1.93	0.0002	9	18.6	74.6
Carrier								
P02089	Hemoglobin subunit beta-2	+1.19	0.0042	−1.28	0.0158	4	22.4	15.9
P07724	Serum albumin	+1.02	0.0006	---	---	26	45.7	68.7
P02088	Hemoglobin subunit beta-1	+0.94	0.0222	−1.29	0.0245	11	83.0	15.8
Carbohydrate metabolism								
P06151	L-lactate dehydrogenase A chain	+1.19	0.0005	+0.70	0.0387	10	28.3	36.5
Q05920	Pyruvate carboxylase, mitochondrial[a]	+1.11	0.0301	−0.68	0.0435	15	14.6	129.7
Q8VC30	Bifunctional ATP-dependent	+0.86	0.0030	−0.96	0.0123	6	17.1	59.7
P16858	Glyceraldehyde-3-phosphate dehydrogenase[a]	+0.81	0.0084	---	---	8	32.4	35.8
P97328	Ketohexokinase[a]	+0.76	0.0074	---	---	2	10.7	32.8
P09411	Phosphoglycerate kinase 1[a]	+0.75	0.0181	---	---	8	28.5	44.6
P40142	Transketolase[a]	+0.67	0.0004	---	---	6	14.1	67.6
Q64442	Sorbitol dehydrogenase[a]	---	---	−0.88	0.0127	9	32.2	38.2
O70475	UDP-glucose 6-dehydrogenase[a]	---	---	−1.34	0.0031	2	4.7	54.8
Chaperones								
P14211	Calreticulin	+1.22	0.0050	+1.17	0.0093	9	31.5	48.0
Q64433	10 kDa heat shock protein, mitochondrial[a]	+0.89	0.0137	−0.63	0.0226	4	45.1	11.0
P20029	78 kDa glucose-regulated protein	+0.89	0.0056	---		19	33.9	72.4
P08113	Endoplasmin[a]	+0.89	0.0030	+0.93	0.0043	16	24.8	92.5
P08003	Protein disulfide-isomerase A4	+0.87	0.0036	---	---	5	11.3	72.0
P63038	60 kDa heat shock protein, mitochondrial	+0.81	0.0061	---	---	13	25.1	61.0
P63017	Heat shock cognate 71 kDa protein	+0.73	0.0264	---	---	15	31.9	70.9
Q61316	Heat shock 70 kDa protein 4	+0.72	0.0283	---	---	6	10.0	94.1
P80318	T-complex protein 1 subunit gamma[a]	+0.66	0.0211	---	---	5	10.5	60.6

Table 1 (*continued*)

ID UniProtKB	Protein name	5 weeks of infection Log_2 (maxLFQ ratio) Test/Control	5 weeks of infection p value	7 weeks of infection Log_2 (maxLFQ ratio) Test/Control	7 weeks of infection p value	Razor + unique peptides	Unique + razor sequence coverage [%]	Mol. weight [kDa]
P27773	Protein disulfide-isomerase A3[a]	+0.48	0.0171	---	---	14	28.7	56.7
P11499	Heat shock protein HSP 90-beta	---	---	+0.50	0.0190	18	27.8	83.3
P38647	Stress-70 protein, mitochondrial[a]	---	---	−0.91	0.0451	12	24.7	73.5
Energy metabolism								
P08249	Malate dehydrogenase, mitochondrial	+1.05	0.0119	---		10	41.1	35.6
P97807-27	Isoform Cytoplasmic of Fumarate hydratase[a]	+0.99	0.0007	−0.59	0.0111	3	9.2	50.1
Q8QZT1	Acetyl-CoA acetyltransferase, mitochondrial	+0.97	0.0070	−0.77	0.0215	6	21.9	44.8
O08749	Dihydrolipoyl dehydrogenase, mitochondrial[a]	+0.61	0.0001	---	---	3	7.1	54.3
Q03265	synthase subunit alpha, mitochondrial[a]	+0.61	0.0211	---	---	6	15.4	59.8
P14152	Malate dehydrogenase, cytoplasmic	---	---	−0.81	0.0243	7	24.0	36.5
P56480	ATP synthase subunit beta, mitochondrial	---	---	−0.84	0.0188	13	35.5	56.3
Stress								
P00329	Alcohol dehydrogenase 1[a]	+1.37	0.0000	−0.72	0.0254	9	44.8	39.8
P99029-29	Peroxiredoxin-5, mitochondrial[a]	+1.26	0.0048	---	---	6	46.9	17.0
P28474	Alcohol dehydrogenase class-3[a]	+1.01	0.0001	---	---	7	21.7	39.5
P34914	Bifunctional epoxide hydrolase 2[a]	+0.95	0.0112	---	---	6	19.1	62.5
P19157	Glutathione S-transferase P1	+0.85	0.0078	---	---	4	28.6	23.6
P11352	Glutathione peroxidase 1[a]	+0.84	0.0005	−1.38	0.0007	7	37.8	22.3
P35700	Peroxiredoxin-1	+0.83	0.0025	−0.83	0.0030	8	43.2	22.2
P16015	Carbonic anhydrase 3	+0.73	0.0001	---	---	10	46.9	29.4
O08709	Peroxiredoxin-6	+0.68	0.0241	−1.21	0.0003	9	46.0	24.9
Q8R086	Sulfite oxidase, mitochondrial[a]	+0.63	0.0067	−1.41	0.0085	3	8.1	60.8
P24270	Catalase	+0.58	0.0381	−1.73	0.0051	16	34.2	59.8
Q8BH00	Aldehyde dehydrogenase family 8 member A1[a]	---	---	−0.62	0.0374	10	33.7	53.7
P47738	Aldehyde dehydrogenase, mitochondrial	---	---	−0.78	0.0109	17	42.8	56.5
P48758	Carbonyl reductase [NADPH] 1[a]	---	---	−0.88	0.0305	7	26.7	30.6
P08228	Superoxide dismutase [Cu-Zn]	---	---	−0.74	0.0168	4	29.9	15.9
P30115	Glutathione S-transferase A3[a]	---	---	−0.84	0.0390	7	28.1	25.4
P10649	Glutathione S-transferase	---	---	−0.92	0.0179	8	36.2	26.0
O08807	Peroxiredoxin-4[a]	---	---	−1.32	0.0013	2	9.1	31.1
P24549	Retinal dehydrogenase 1[a]	---	---	−1.41	0.0002	12	34.1	54.5
Structural								
P05784	Cytokeratin18	+1.46	0.0313	+1.03	0.0108	10	25.8	47.5
P21107-2	Isoform 2 of Tropomyosin alpha-3 chain	+1.43	0.0145	---	---	4	15.3	29.0
P20065-2	Isoform Short of Thymosin beta-4[a]	+1.23	0.0176	---	---	3	61.4	5.1
P11679	Cytokeratin8	+1.20	0.0001	+1.29	0.0095	8	17.1	54.6
P18760	Cofilin-1[a]	+1.01	0.0424	---	---	5	41.0	18.6
Q60715-2	Isoform 2 of Prolyl 4-hydroxylase subunit alpha-1	+0.52	0.0128	---	---	3	6.4	60.9
P62962	Profilin-1[a]	---	---	+1.40	0.0233	6	47.9	15.0
O89053	Coronin-1A[a]	---	---	−1.37	0.0078	2	5.4	51.0
Immune system								
E9PV24	Fibrinogen alpha chain[a]	+0.89	0.0012	---	---	2	4.3	61.3
P01868	Ig gamma-1 chain C region secreted form[a]	+0.75	0.0166	---	---	2	6.8	35.7
Lipid metabolism								
Q61578	NADPH:adrenodoxin oxidoreductase, mitochondrial[a]	+1.98	0.0356	---	---	2	5.3	54.2
P45952	Medium-chain specific acyl-CoA dehydrogenase[a]	+1.19	0.0011	---	---	5	15.0	46.5
Q07417	Short-chain specific acyl-CoA dehydrogenase[a]	+1.18	0.0253	−1.15	0.0333	4	16.3	44.9
P10518	Delta-aminolevulinic acid dehydratase[a]	+1.02	0.0010	---	---	6	27.3	36.0
Q8BWT1	3-ketoacyl-CoA thiolase, mitochondrial [a]	+0.97	0.0015	---	---	11	37.0	41.8
P06801	NADP-dependent malic enzyme[a]	+0.87	0.0010	---	---	2	4.4	64.0
P19096	Fatty acid synthase	+0.68	0.0440	−1.59	0.0107	10	6.2	272.4
P31786	Acyl-CoA-binding protein[a]	−0.48	0.0496	---	---	3	36.8	10.0
P54869	Hydroxymethylglutaryl-CoA	---	---	−0.70	0.0387	10	26.0	56.8

(*continued on next page*)

Table 1 (*continued*)

ID UniProtKB	Protein name	5 weeks of infection Log_2 (maxLFQ ratio) Test/Control	5 weeks of infection p value	7 weeks of infection Log_2 (maxLFQ ratio) Test/Control	7 weeks of infection p value	Razor + unique peptides	Unique + razor sequence coverage [%]	Mol. weight [kDa]
	synthase, mitochondrial[a]							
Nucleotide metabolism								
P25688	Uricase[a]	+1.40	0.0024	---	---	11	36.6	35.0
P00375	Dihydrofolate reductase[a]	+1.23	0.0020	---	---	2	13.9	21.6
Q01768	Nucleoside diphosphate kinase B	+0.60	0.0029	---	---	6	35.5	17.4
Carbon metabolism								
Q8R0Y6	Cytosolic 10-formyltetrahydrofolate dehydrogenase[a]	+0.85	0.0001	−1.05	0.0064	25	39.5	98.7
Other processes								
O88587-2	Catechol *O*-methyltransferase[a]	+1.59	0.0108	---	---	2	14.9	24.7
O08795-2	Glucosidase 2 subunit beta[a]	+1.18	0.0082	---	---	4	8.8	58.8
O88587	Catechol *O*-methyltransferase[a]	+0.83	0.0026	---	---	2	14.9	24.7
P52196	Thiosulfate sulfurtransferase[a]	+0.70	0.0488	−0.53	0.0176	9	35.4	33.5
Q64105	Sepiapterin reductase[a]	---	---	−0.87	0.0335	4	24.1	27.9
Protease								
P10605	Cathepsin B[a]	+1.10	0.0108	---	---	5	18.9	37.3
Signaling								
P61982	14-3-3 protein gamma[a]	+1.38	0.0006	---	---	3	17.4	28.3
O35887	Calumenin	+1.37	0.0090	---	---	5	20.0	37.1
P63101	14-3-3 protein zeta/delta	+1.20	0.0195	---	---	7	39.6	27.8
P70296	Phosphatidylethanolamine-binding protein 1[a]	+1.06	0.0171	−0.51	0.0332	6	57.8	20.8
P11276	Fibronectin[a]	+0.84	0.0009	---	---	4	2.3	272.5
Q64374	Regucalcin[a]	+0.81	0.0313	−1.11	0.0032	15	61.2	33.4
O55023	Inositol monophosphatase 1[a]	---	---	+0.36	0.0087	2	7.2	30.4
Translation								
Q91VI7	Ribonuclease inhibitor	+1.03	0.0002	---	---	5	16.4	49.8
P99027	60S acidic ribosomal protein P2[a]	+0.69	0.0057	---	---	4	53.0	11.7
P60843	Eukaryotic initiation factor 4A-I[a]	+0.67	0.0010	---	---	5	16.7	46.2
P52760	Ribonuclease UK114[a]	+0.58	0.0013	−1.79	0.0058	6	65.2	14.3
P58252	Elongation factor 2	---	---	+0.52	0.0171	12	16.7	95.3
Transcription								
P02301	Histone H3.3C[a]	+0.87	0.0071	---	---	2	11.8	15.3
O35737	Heterogeneous nuclear ribonucleoprotein H[a]	+0.85	0.0208	−1.13	0.0011	3	11.1	49.2
P62806	Histone H4[a]	+0.54	0.0078	---	---	3	29.1	11.4
Transport								
Q68FD5	Clathrin heavy chain 1[a]	+1.08	0.0099	---	---	9	8.1	191.6

The identified proteins were classified according to their biological function using Gene ontology (GO) and UniProtKB databases. Log_2 (maxLFQ) ratio ≥ 1 corresponds to a 2-fold increase in abundance. (+) indicates increase in abundance whereas (−) indicates decrease in abundance. (−) indicates protein not identified/quantified in a particular group.

[a] Novel proteins found at altered levels in the Balb/c model of schistosomiasis. Protein names were listed as recommended by UniProt Knowledgebase – UniProtKB.

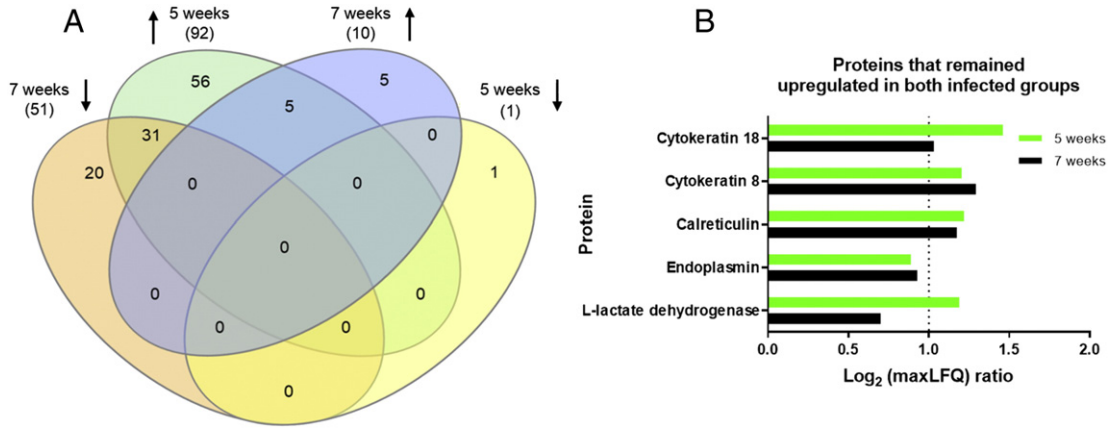

Fig. 3. Few proteins persist up-regulated in the liver of Balb/c infected mice during hepatosplenic schistosomiasis. A - Venn diagram illustrating the number of proteins found in each stage of the disease and those that were shared. Upward pointing arrows correspond to up-regulation of proteins whilst downward pointing arrows illustrate down-regulation. Numbers in brackets represent the sum of proteins from each group. B - Only five proteins remained at significantly increased levels along the 5th and 7th weeks post infection. Note that Log_2 (maxLFQ) ratio = 1 corresponds to a 2-fold increase in protein abundance.

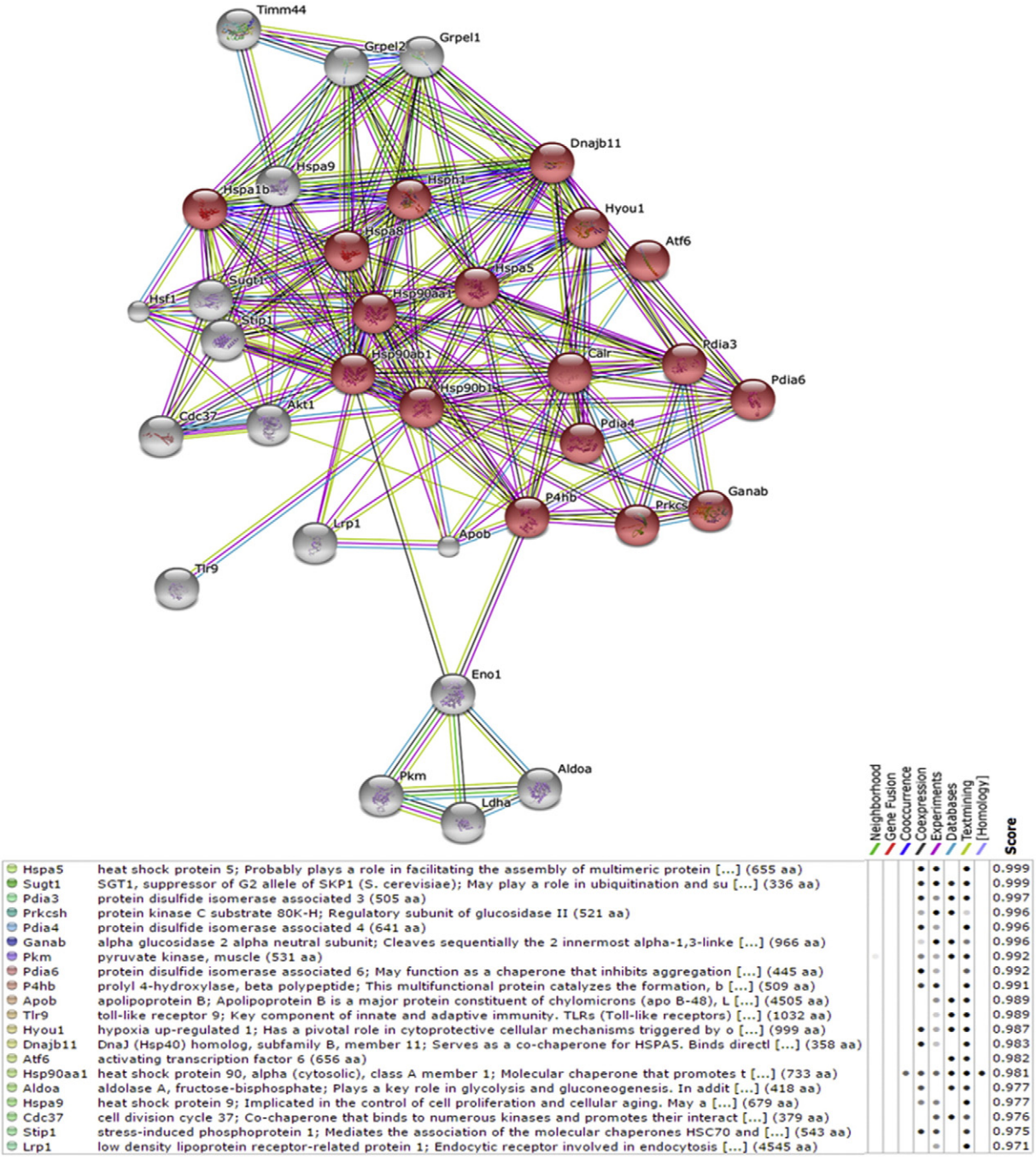

Fig. 4. Protein interaction network. Three proteins (Carl – calreticulin, Hsp90b1 – endoplasmin and Ldha – lactate dehydrogenase A) found to be up-regulated at 5 and 7 weeks of infection were used as inputs to build up an interaction network using the STRING v10 algorithm. Then, the 20 most highly connected nodes were requested (see frame for nomenclature of predicted functional partners). Red nodes illustrate interacting proteins known to have a role in protein quality control at the endoplasmic reticulum.

Gene ontology categorization revealed many of these proteins involved in various cellular processes such as metabolism, stress, structural maintenance, immune response, and signaling. It is worth emphasizing that the 5th week post infection in the Balb/c model is characterized by the presence of mainly immature eggs in the liver parenchyma around which a granulomatous inflammation, induced by egg-released antigens, had just been triggered. At this point, splenomegaly has been established and the liver of infected Balb/c mice revealed very active at up-regulating the levels of several molecules. Among the quantified proteins at this stage the urea cycle constituents were quite prominent indicating the need to detoxify ammonia into urea as a result of an increase in amino acid metabolism [22,23]. Such an enhanced amino acid processing in the liver can also be explained by the high demand of protein synthesis, in particular of collagen to sustain granuloma formation. In this scenario the high levels of mitochondrial glutamate dehydrogenase was expected as this enzyme is actively involved in the conversion of glutamate into proline, the latter of known abundance in collagen. In agreement, the oxygen sensor enzyme prolyl-4-hydroxylase (PHD), which catalyses proline hydroxylation as a requisite for triple helix formation of collagens, was found significantly up-regulated, corroborating with a previously reported study [5]. Such an unusual rate of proline hydroxylation might compromise hydroxylation of other known protein substrates of PHD, such as hypoxia-inducible factor, leading to its stabilization in the cytosol [24,25]. This in turn

might explain the consequent increase in anaerobic metabolism in the hepatic tissue. A testimonial of that important metabolic alteration is the observed >2-fold increase in abundance of lactate dehydrogenase. In fact, metabolomic investigations have revealed increased levels of lactate in the liver of 5 week-infected Balb/c mice [7].

As the infection progresses to the chronic phase, fully developed eggs are likely to become more competent at releasing parasite antigens in the liver tissue leading to a pronounced inflammation and consequently to major hepatotoxicity [26,27]. Indeed, the soluble liver proteome at 7 weeks post infection, was largely dominated by down-regulation of proteins. It is worth emphasizing that our stringent criteria for protein quantification probably excluded most of the proteins uniquely expressed by inflammatory cells, as they were not detected in the control samples or their corresponding levels were too low to be accurately quantified. Therefore, we believe the down-regulation of proteins seen at the chronic phase is predominantly a response of hepatocytes to the infection. Among the 61 proteins significantly altered, only 10 proteins exhibited up-regulation, these included chaperonins and structural proteins. Calreticulin and endoplasmin, two known constituents involved in protein folding at the endoplasmic reticulum, alongside the cytosolic HSP90-β were found at high levels. Two other proteins of interest glutamine γ-glutamyltransferase and L-lactate dehydrogenase, also showed higher expression in the hepatosplenic phase of the disease. Cytokeratins (K8 and K18) and profilin-1, a known regulator of cytoskeleton organization [28,29] are representatives of structural proteins that remained at high abundance, reaching >2 fold increase in chronic murine schistosomiasis.

It is of note that cytokeratins (K8 and K18), calreticulin, endoplasmin and L-lactate dehydrogenase were the only five proteins found in this study to remain at high levels (>2 fold increase as judged by MaxQuant) during splenic and hepatosplenic schistosomiasis. Cytokeratins are constituents of intermediate filaments, often occurring in pairs comprising of type I and type II cytokeratins [30,31]. Aside from their structural function these molecules have been shown to perform key roles in signaling, stress response, apoptosis and cell migration [32,33]. The specific tissue distribution of K8 and K18 keratins has instigated their potential use as biomarkers of liver disorders [34,35]. In fact, K18 is differentially expressed in the livers of *S. mansoni* -infected animals and its presence in serum has been evaluated as a potential marker of infection by this parasite [6].

The remaining three proteins exhibiting persistent high levels in the two stages of the disease, calreticulin, endoplasmin and L-lactate dehydrogenase were then selected as entries to build up a protein interaction network using the STRING algorithm. Analysis of the 20 most highly connected partners allowed easy observation of two major cellular processes operating in the diseased liver tissue. Firstly, a stress response in the endoplasmic reticulum (ER) is evident as in parallel to calreticulin and endoplasmin (labeled as Hsp90b1 in the network) [36,37], further additional 15 interactors made up a high confidence network composed mostly of chaperones. Possibly, this is a result of high demand in protein quality control in that compartment with consequent recovery of misfolded proteins or their destination to degradation via ERAD [38,39]. Corroborating our experimental data, major players in the response to hypoxia, such as hypoxia up-regulated protein 1 (Hyou1), protein disulfide-isomerase A3, protein disulfide-isomerase A4 and prolyl-4 hydroxylase (P4hb), the last three differentially identified in our study, showed up as strong interactors in the network. In fact, enolase 1 (eno1) a known target gene of the response to hypoxia [40,41] made up the missing link between the endoplasmic reticulum constituents and the increase in glycolytic enzymes in the cytosol, including lactate dehydrogenase. The metabolic alterations seen in the liver during chronic schistosomiasis could ultimately lead to prohibitive low levels of intra-hepatic ATP, hence contributing to irreversible organ failure and to foreseeable death of the vertebrate host.

It is important to emphasize that the proteomic alterations observed in our investigation are in good agreement with those previously reported by Manivannan et al. [5], in which a 2D-DIGE approach was employed. However, considering the commonalities observed, fold alterations are not directly comparable as the former study relied on quantification based on protein spot volume and only changes exhibiting >2fold increase or decrease in expression were reported. Moreover, a different mouse strain was used in that study and most of their findings are related to proteomic alterations observed by comparing non-infected animals with those exhibiting the pre hepatosplenic schistosomiasis. Composing the list of proteins that exhibited fold discrepancies between these two studies are some molecules involved in amino acid metabolism and stress response, such as glutamate dehydrogenase, carbamoyl phosphate synthase and glutathione S-transferase P1.

We believe the novel set of proteins presented in this shotgun analysis greatly expanded our understanding on the establishment of liver disease caused by *S. mansoni*. In parallel, it opened up new perspectives for searching biomarkers that could aid in early diagnosis to favor treatment and prevent the chronic and often irremediable complications of this condition.

5. Conclusions

In this work we conducted a quantitative shotgun proteomic analysis of the liver soluble proteome of *S. mansoni*-infected Balb/c mice during splenic and hepatosplenic schistosomiasis. Our data revealed the former stage dominated by up-regulation of molecules at the 5th post infection, coincident with the onset of oviposition. In stark contrast, the proteome of chronically infected liver revealed predominantly down-regulation of molecules with few classic representatives, involved in endoplasmic reticulum stress and anaerobic metabolism, maintained at persistent high levels.

Supplementary data to this article can be found online at http://dx.doi.org/10.1016/j.jprot.2016.07.013.

Authors' contributions

JMC, LXN, NCNP, RAOC performed the experiments. All the listed authors designed the experiments and analysed the data. JMC, LXN and WCB wrote the manuscript.

Conflicts of interest

None declared.

Transparency document

The Transparency document associated with this article can be found, in the online version.

Funding sources

This work was financially supported by 'Fundação de Amparo à Pesquisa do Estado de Minas Gerais' (FAPEMIG, grant number APQ-02660-10) and 'Coordenação de Aperfeiçoamento de Pessoal de Nível Superior' (CAPES – grant number 170/2012). Complementary research fundings were also obtained from UFOP (grant numbers: 23109.006271/2014-70 and 23109.003753/2015-59). JMC was a recipient of a CAPES scholarship for the funding of his MSc degree in Biotechnology.

References

[1] Y. Lu, et al., Identification and profiling of circulating antigens by screening with the sera from schistosomiasis japonica patients, Parasit Vectors 5 (2012) 115.
[2] D. Wichmann, et al., Diagnosing schistosomiasis by detection of cell-free parasite DNA in human plasma, PLoS Negl. Trop. Dis. 3 (4) (2009), e422.

[3] F.R. Martins-Melo, et al., Trends in schistosomiasis-related mortality in Brazil, 2000–2011, Int. J. Parasitol. 44 (14) (2014) 1055–1062.
[4] M. Harvie, T.W. Jordan, A.C. La Flamme, Differential liver protein expression during schistosomiasis, Infect. Immun. 75 (2) (2007) 736–744.
[5] B. Manivannan, et al., Proteomic changes at 8 weeks after infection are associated with chronic liver pathology in experimental schistosomiasis, J. Proteome 75 (6) (2012) 1838–1848.
[6] B. Manivannan, et al., Identification of cytokeratin 18 as a biomarker of mouse and human hepatosplenic schistosomiasis, Infect. Immun. 79 (5) (2011) 2051–2058.
[7] J. Wu, et al., Metabolic changes reveal the development of schistosomiasis in mice, PLoS Negl. Trop. Dis. (2010) 4(8).
[8] C.I. Balog, et al., Metabonomic investigation of human *Schistosoma mansoni* infection, Mol. BioSyst. 7 (5) (2011) 1473–1480.
[9] S.R. Smithers, R.J. Terry, The infection of laboratory hosts with cercariae of *Schistosoma mansoni* and the recovery of the adult worms, Parasitology 55 (4) (1965) 695–700.
[10] R.H. Duvall, W.B. DeWitt, An improved perfusion technique for recovering adult schistosomes from laboratory animals, Am.J.Trop. Med. Hyg. 16 (4) (1967) 483–486.
[11] G.S. Henderson, et al., Two distinct pathological syndromes in male CBA/J inbred mice with chronic *Schistosoma mansoni* infections, Am. J. Pathol. 142 (3) (1993) 703–714.
[12] J. Cox, M. Mann, MaxQuant enables high peptide identification rates, individualized p.p.b.-range mass accuracies and proteome-wide protein quantification, Nat. Biotechnol. 26 (12) (2008) 1367–1372.
[13] J. Cox, et al., Accurate proteome-wide label-free quantification by delayed normalization and maximal peptide ratio extraction, termed MaxLFQ, Mol. Cell. Proteomics 13 (9) (2014) 2513–2526.
[14] B. Schilling, et al., Platform-independent and label-free quantitation of proteomic data using MS1 extracted ion chromatograms in skyline: application to protein acetylation and phosphorylation, Mol. Cell. Proteomics 11 (5) (2012) 202–214.
[15] D. Szklarczyk, et al., STRING v10: protein-protein interaction networks, integrated over the tree of life, Nucleic Acids Res. 43 (Database issue) (2015) D447–D452.
[16] B. Manivannan, et al., Differential patterns of liver proteins in experimental murine hepatosplenic schistosomiasis, Infect. Immun. 78 (2) (2010) 618–628.
[17] M. Mann, et al., The coming age of complete, accurate, and ubiquitous proteomes, Mol. Cell 49 (4) (2013) 583–590.
[18] Q. Hu, et al., The Orbitrap: a new mass spectrometer, J. Mass Spectrom. 40 (4) (2005) 430–443.
[19] N. Nagaraj, et al., System-wide perturbation analysis with nearly complete coverage of the yeast proteome by single-shot ultra HPLC runs on a bench top Orbitrap, Mol Cell Proteomics 11 (3) (2012) M111 013722.
[20] D. Chelius, P.V. Bondarenko, Quantitative profiling of proteins in complex mixtures using liquid chromatography and mass spectrometry, J. Proteome Res. 1 (4) (2002) 317–323.
[21] K.A. Neilson, et al., Label-free quantitative shotgun proteomics using normalized spectral abundance factors, Methods Mol. Biol. 1002 (2013) 205–222.
[22] C. Spanaki, A. Plaitakis, The role of glutamate dehydrogenase in mammalian ammonia metabolism, Neurotox. Res. 21 (1) (2012) 117–127.
[23] L. Jin, et al., Glutamate dehydrogenase 1 signals through antioxidant glutathione peroxidase 1 to regulate redox homeostasis and tumor growth, Cancer Cell 27 (2) (2015) 257–270.
[24] K.J. Nytko, et al., Regulated function of the prolyl-4-hydroxylase domain (PHD) oxygen sensor proteins, Antioxid. Redox Signal. 9 (9) (2007) 1329–1338.
[25] H. Boulahbel, R.V. Duran, E. Gottlieb, Prolyl hydroxylases as regulators of cell metabolism, Biochem. Soc. Trans. 37 (Pt 1) (2009) 291–294.
[26] M.H. Abdulla, et al., Proteomic identification of IPSE/alpha-1 as a major hepatotoxin secreted by *Schistosoma mansoni* eggs, PLoS Negl. Trop. Dis. 5 (10) (2011), e1368.
[27] W. Mathieson, R.A. Wilson, A comparative proteomic study of the undeveloped and developed *Schistosoma mansoni* egg and its contents: the miracidium, hatch fluid and secretions, Int. J. Parasitol. 40 (5) (2010) 617–628.
[28] M. Pae, G.R. Romeo, The multifaceted role of profilin-1 in adipose tissue inflammation and glucose homeostasis, Adipocyte 3 (1) (2014) 69–74.
[29] F. Bordeleau, et al., Keratin 8/18 regulation of cell stiffness-extracellular matrix interplay through modulation of rho-mediated actin cytoskeleton dynamics, PLoS One 7 (6) (2012), e38780.
[30] J. Schweizer, et al., New consensus nomenclature for mammalian keratins, J. Cell Biol. 174 (2) (2006) 169–174.
[31] R. Moll, M. Divo, L. Langbein, The human keratins: biology and pathology, Histochem. Cell Biol. 129 (6) (2008) 705–733.
[32] T. Busch, et al., Keratin 8 phosphorylation regulates keratin reorganization and migration of epithelial tumor cells, J. Cell Sci. 125 (Pt 9) (2012) 2148–2159.
[33] C.M. Alam, et al., Keratin 8 modulates beta-cell stress responses and normoglycaemia, J. Cell Sci. 126 (Pt 24) (2013) 5635–5644.
[34] N.O. Ku, et al., Keratin 8 and 18 mutations are risk factors for developing liver disease of multiple etiologies, Proc. Natl. Acad. Sci. U. S. A. 100 (10) (2003) 6063–6068.
[35] P.A. Coulombe, M.B. Omary, 'hard' and 'soft' principles defining the structure, function and regulation of keratin intermediate filaments, Curr. Opin. Cell Biol. 14 (1) (2002) 110–122.
[36] J. Khalife, et al., Cloning of the gene encoding a *Schistosoma mansoni* antigen homologous to human Ro/SS-A autoantigen, Mol. Biochem. Parasitol. 57 (2) (1993) 193–202.
[37] Z. Yang, et al., Upregulation of heat shock proteins (HSPA12A, HSP90B1, HSPA4, HSPA5 and HSPA6) in tumour tissues is associated with poor outcomes from HBV-related early-stage hepatocellular carcinoma, Int J Med Sci 12 (3) (2015) 256–263.
[38] A. Stolz, D.H. Wolf, Endoplasmic reticulum associated protein degradation: a chaperone assisted journey to hell, Biochim. Biophys. Acta 1803 (6) (2010) 694–705.
[39] L. Dara, C. Ji, N. Kaplowitz, The contribution of endoplasmic reticulum stress to liver diseases, Hepatology 53 (5) (2011) 1752–1763.
[40] G.L. Semenza, et al., Hypoxia response elements in the aldolase A, enolase 1, and lactate dehydrogenase A gene promoters contain essential binding sites for hypoxia-inducible factor 1, J. Biol. Chem. 271 (51) (1996) 32529–32537.
[41] M. Capello, et al., Alpha-enolase: a promising therapeutic and diagnostic tumor target, FEBS J 278 (7) (2011) 1064–1074.